ELSEVIER

Journal of Power Sources 63 (1996) 93–96

JOURNAL OF POWER SOURCES

Electrochemical behaviour of vanadium bronze $Li_6V_5O_{15}$ cathode in a secondary lithium battery

Shouhan Hua, Guolun Zhong, Nengzuo Jiang

Department of Chemistry, Shandong University, Jinan 250100, People's Republic of China

Received 17 April 1996; accepted 27 June 1996

Abstract

A new vanadium oxide that is rich in lithium ($Li_6V_5O_{15}$) has been prepared from Li_2CO_3 and V_2O_5 at 680 °C for 24 h. The discharge behaviour of the bronze electrode is investigated in an $Li/LiAsF_6$–PC/bronze battery at various current densities. The new material has good reversibility for lithium insertion; a high specific capacity (more than 340 Ah kg^{-1}) is obtained at 0.2 mA cm^{-2} and a 1.0 V cutoff voltage. Given the good structural stability of the bronze with Li^+ insertion, 160 cycles are achieved with the tentative battery. A.c. impedance data for the $Li/Li_6V_5O_{15}$ cell reveal that the cathodic process is controlled mainly by Li^+ diffusion in the bronze. The new bronze could be used for a low-voltage, rechargeable lithium battery.

Keywords: Vanadium bronze; Secondary lithium batteries; Lithium insertion reaction; A.c. impedance; X-ray diffraction

1. Introduction

Numerous studies of positive electrode materials for secondary lithium batteries have been carried out during the past couple of decades. Many transition metal oxides or their mixtures, such as vanadium oxides, V_6O_{13}, $Li_{1+x}V_3O_8$, MnO_2–V_2O_5, NiO–V_2O_5 [1–3], have been recommended for such electrode materials. The V_6O_{13} has a high specific energy, but it cannot withstand over-discharge. Though $Li_{1+x}V_3O_8$ can be easily synthesized in air, its specific energy is insufficient.

The $Li_{1+x}V_3O_8$ bronze has been investigated with electrochemical methods by Ponero et al. [4]. The results showed that at high Li^+ concentration, poor charge screening produces a remarkable Li^+–Li^+ repulsion due to electron localization [5]. The influence of a high Li/V ratio on the electrochemical characteristics of the vanadium bronze has not been reported. This study discloses the preparation of a new kind of vanadium bronze that is rich in lithium, together with the electrochemical behaviour of this material in a secondary lithium battery.

2. Experimental

By heating a 3:4 mixture of V_2O_5 and Li_2CO_3 at 680 °C in air for 24 h, a substance was obtained and then dissolved in hot water. By filtering the solution to remove the insoluble solid, evaporating, and heating the viscous concentrated solution at about 120 °C for 2–3 h, a yellowish vanadium bronze was prepared.

The $LiAsF_6$ was used as received, but the $LiClO_4$ (AR grade) was dried under vacuum at 160–180 °C for 20 h and stored in a dry box.

The solvent purification procedures for propylene carbonate (PC), dimethoxyethane (DME), and 2-methyltetrahydrofuran (2Me-THF) were the same as those reported previously [6]. PC was distilled under reduced pressure (400 Pa) and the middle fraction was collected for use.

The positive electrode was prepared by pressing a mixture of the new vanadium bronze, acetylene black and polytetrafluoroethylene (PTFE) in a weight ratio of 5:1:1 onto a 80-mesh nickel net at 300 kg cm^{-2}. Lithium foil, pressed onto the nickel net, served as a negative electrode.

The test cell was assembled in a dry box and comprised one positive electrode wrapped in Celgard 2400-5511 membranes, and two negatives. Cycling experiments were performed with an AMEL 545-galvanostat-electrometer. A Solartron 1250 frequency response analyser was used to measure the a.c. impedance of the cell.

3. Results and discussion

Chemical analysis of the material indicated that the bronze contained 90 wt.% $Li_2O \cdot V_2O_5$ and 10 wt.% $3Li_2O \cdot V_2O_5$, and the mole ratio of Li/V was 1.2, and that no V^{4+} was

PII S0378-7753(96)02451-2

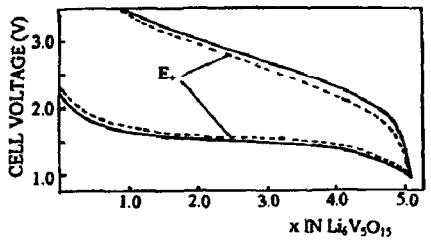

Fig. 1. Discharge curves of Li/1 mol l^{-1} $LiAsF_6$–PC/$Li_6V_5O_{15}$ cell at first cycle, $i_c = i_d = 1.0$ mA cm^{-2}; E_+ = potential of positive electrode vs. lithium.

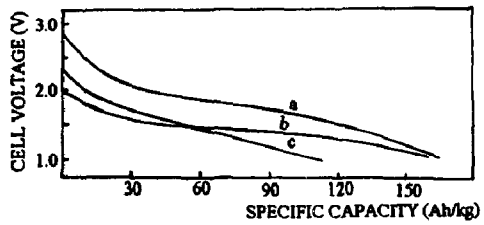

Fig. 2. Discharge curves of Li/1 mol l^{-1} $LiAsF_6$–PC–DME/$Li_6V_5O_{15}$ cell at different current densities: (a) $i_{d2} = 1.0$ mA cm^{-2} (second); (b) $i_{d1} = 2.0$ mA cm^{-2} (first), and (c) $i_{d3} = 3.0$ mA cm^2 (third).

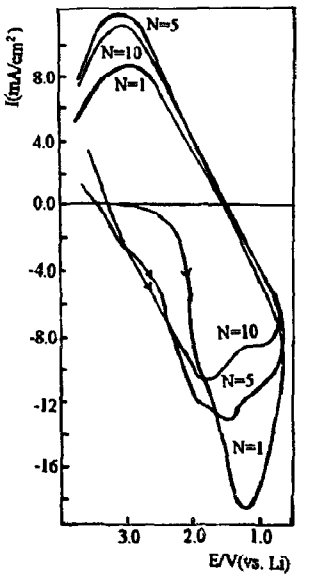

Fig. 3. Cyclic voltammograms of Li/1 mol l^{-1} $LiAsF_6$–PC/$Li_6V_5O_{15}$ cell between 0.8 and 3.8 V at a scan rate of 2 mV s^{-1}, N: cycling number.

detected. These results are in agreement with the X-ray diffraction data. Thus, the chemical formula of the new vanadium bronze can be expressed approximately as $Li_6V_5O_{15}$.

Typical first charge/discharge curves for the Li/1 mol l^{-1} $LiAsF_6$–PC/$Li_6V_5O_{15}$ cell are given in Fig. 1; the current density of charge/discharge was 1.0 mA cm^{-2}. The Li/$Li_6V_5O_{15}$ cell had smooth discharge curves, the discharge plateau was about 1.6 V, and the open-circuit voltage (OCV) was 3.2 V after assembling. Using a low current rate (0.2 mA cm^{-2}) on the first discharge with a 1.0 V cutoff voltage, nearly 6 moles of lithium can be incorporated into one mole of the bronze ($Li_6V_5O_{15}$); this corresponds to a specific capacity of 340 Ah kg^{-1}. There is little difference in the voltage curves and this indicates that the positive material has a good microstructure for lithium insertion with low polarization. A specific energy of 540 Wh kg^{-1} was obtained with 1 mol l^{-1} $LiAsF_6$–PC electrolyte on the basis of positive-electrode weight. The high charge efficiency (82%) of the cell shows that the vanadium bronze is reversible for lithium intercalation and remains structurally stable. As seen from Fig. 2, the working voltage of the cell increased slightly during the first few cycles and then remained unchanged with further cycling. The material could be over-discharged without damage. In contrast with V_6O_{13}, no voltage plateaus were observed below 1.8 V and an irreversible capacity was found between this value and 1.0 V with breakdown of V–O bonds [7].

The large difference between the voltage plateaus on charge and discharge suggests that the cell reaction may have a high activation energy with a certain phase change. In addition, the new lithium-rich vanadium bronze is not sensitive to moisture; this is an advantage over V_6O_{13} and TiS_2. It is also found that short-circuit or voltage reversal does not cause serious damage to the cell, after several cycles the loss in capacity could be virtually recovered.

The discharge curves of the Li/$Li_6V_5O_{15}$ cell with 1 mol l^{-1} $LiAsF_6$–PC–DME (1:1) electrolyte at different discharge rates are presented in Fig. 2. The smooth discharge curves indicate the single-phase behaviour of the bronze. The results confirm that the $Li_6V_5O_{15}$ has good discharge characteristics with a moderate discharge rate for practical use. Even with a high discharge rate of 3.0 mA cm^{-2}, a capacity of 110 Ah kg^{-1} can be obtained.

Cyclic voltammograms of an $Li_6V_5O_{15}$ electrode in the potential range of 0.8 to 3.8 V (versus Li) at a scan rate of 2 mV s^{-1} are given in Fig. 3. There is a large cathodic peak that corresponds to a long voltage plateau (1.6 V) on the titration curve. With cycling, the commencement of the cathodic peak is shifted from about 2.2 to 3.3 V, but that of the anodic peak remains unchanged. This can be explained by a change in structure of the positive material during cycling, which has been confirmed by X-ray diffraction analysis (Fig. 4). The observed linear relationship between the peak current values (I_p) of anodic or cathodic processes and the square root of the scan rate ($\nu^{1/2}$) indicates that the cell reaction is controlled by diffusion of lithium ions in the vanadium bronze.

The X-ray diffraction pattern of the new, lithium-rich vanadium bronze is presented in Fig. 4(a). The strongest peaks are at d: 4.76, 3.35 and 3.06, strong peaks are at d: 2.76, 2.86 and 2.97, and no peaks of V_6O_{13} and $Li_{1+x}V_3O_8$ are found. According to the phase diagram for the metastable system of Li_2O–V_2O_5 [8], the synthetic product consists of two kinds of crystals, namely, $Li_2O \cdot V_2O_5$ and $3Li_2O \cdot V_2O_5$. This is confirmed by a comparison of the X-ray analysis results for the bronze (see Table 1) [9]. The diffraction peaks of $Li_2O \cdot V_2O_5$ and $3Li_2O \cdot V_2O_5$ can all be found in the X-ray diffraction data of the bronze, but the intensities of the peaks for $Li_2O \cdot V_2O_5$ are higher than those for $3Li_2O \cdot V_2O_5$. The structure of the vanadium bronze is a rhombohedral system that can provide a good environment for lithium intercalation.

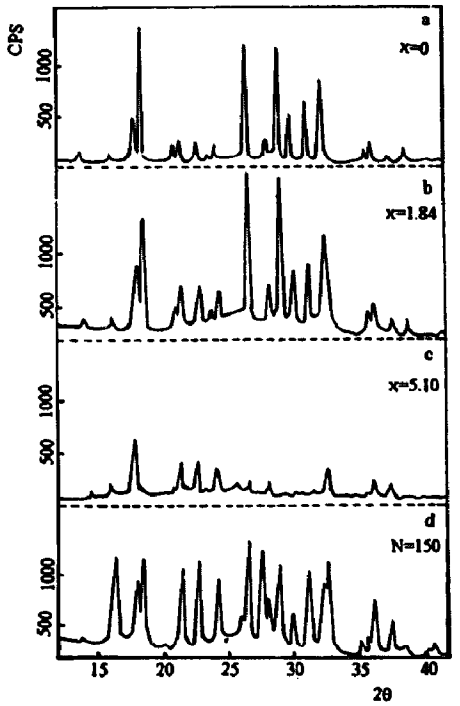

Fig. 4. X-ray diffraction patterns of $Li_6V_5O_{15}$ electrodes, discharged and after cycling.

Table 1
XRD data of $Li_2O \cdot V_2O_5$, $3Li_2O \cdot V_2O_5$ and the new bronze [a]

$Li_2O \cdot V_2O_5$ (I)		$3Li_2O \cdot V_2O_5$ (II)		Vanadium bronze			
				Due to (I)		Due to (II)	
d (Å)	I/I_0	d (Å)	I/I_0	d (Å)	I/I_0	d (Å)	I/I_0
6.35	VW	5.50	VW	6.328	VW	5.470	VW
4.75	VS	4.14	M	4.768	VS	4.134	W
4.21	W	3.90	VS	4.225	W	3.896	W
3.35	VS	3.66	M	3.350	S	3.664	W
3.16	W	3.16	M	3.162	W	3.162	W
3.06	VS	2.74	S	3.062	S	2.740	W
2.97	M	2.48	W	2.969	M	2.470	VW
2.86	M	2.39	M	2.857	M	2.390	VW
2.77	S			2.758	M		
2.50	VW			2.502	VW		

[a] VS: very strong, S: strong, M: middle, W: weak.

The X-ray diffraction patterns of the $Li_6V_5O_{15}$ electrodes after discharging to different depths-of-discharge at 1.0 mA cm^{-2} are shown in Fig. 4. The pattern for the product discharged to 1.5 V ($x = 1.84$, Fig. 4(b)) is very similar to the pattern for an undischarged sample ($x = 0$, Fig. 4(a)), apart from a slight intensification of the $3Li_2O \cdot V_2O_5$ crystal phase. With increasing depth-of-discharge, the intensity of the peaks of the $3Li_2O \cdot V_2O_5$ crystal phase increases gradually, at same time those of $Li_2O \cdot V_2O_5$'s decrease. At $x = 5.10$ (Fig. 4(c)), the peaks of the $Li_2O \cdot V_2O_5$ crystal phase almost disappear and only the peaks of $3Li_2O \cdot V_2O_5$ remain. This indicates that the $Li_2O \cdot V_2O_5$ crystal phase is partly transformed to the $3Li_2O \cdot V_2O_5$ crystal phase when massive amounts of Li^+ ions are inserted into the lattice. The $Li_2O \cdot V_2O_5$ crystal phase can be recovered, however, by recharging. The diffraction peaks of $Li_2O \cdot V_2O_5$ and $3Li_2O \cdot V_2O_5$ are present in the $Li_6V_5O_{15}$ positive electrode in the charged state after 150 cycles (Fig. 4(d)). The relative intensity of the peaks is obviously changed, but no new peaks have appeared.

The discharge behaviour of the Li/$Li_6V_5O_{15}$ cells in different electrolytes at the same discharge rate (1.0 mA cm^{-2}) and to the same cutoff voltage (1.0 V) were investigated. The Li/vanadium bronze cell with 1 mol l^{-1} $LiAsF_6$–PC–DME (1:1) gave the highest OCV (about 3.33 V). As shown in Fig. 5, the highest specific capacity was obtained in 1 mol l^{-1} $LiAsF_6$–2Me–THF [10]. The difference in the capacities of the Li/$Li_6V_5O_{15}$ cells with different electrolytes can be attributed to several factors, for example, solvent co-intercalation, ion solvation and solvent decomposition.

The cycling capacity of an Li/$Li_6V_5O_{15}$ cell at a charge/discharge rate of 1.0/2.0 mA cm^{-2} between 3.5 and 1.0 V is shown in Fig. 6. The capacity falls significantly during the first few cycles but then reaches a stable value after 10 cycles.

The complex impedance plane plots of the Li/1 mol l^{-1} $LiAsF_6$–PC/$Li_6V_5O_{15}$ cell over the frequency range 0.05 to 65 000 Hz with an a.c. signal amplitude of 5 mV in the discharge and recharge processes are given in Fig. 7. In these plots, both kinetically controlled (semi-circular) and diffusion controlled (linear) regions are displayed. The semicircles in Fig. 7 reflect the reaction of the negative electrode/electrolyte interface, the low-frequency part of the complex impedance plot is connected with the diffusion in both the negative and positive electrode interfaces, but the diffusion of lithium in positive electrode exerts a dominant role.

The equivalent circuit of the Li/$Li_6V_5O_{15}$ cell is shown in Fig. 8 [11]. The plot of a.c. complex impedance of this circuit

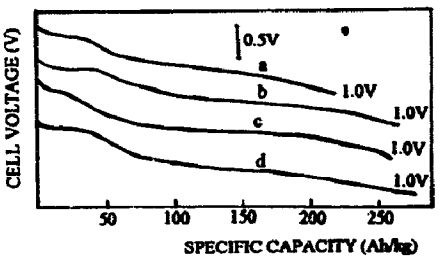

Fig. 5. Voltage profiles of Li/$Li_6V_5O_{15}$ cells in various electrolytes, $i_d = 1.0$ mA cm^{-2}: (a) 1 mol l^{-1} $LiAsF_6$–PC; (b) 1 mol l^{-1} $LiAsF_6$–PC–DME (1:1); (c) 1 mol l^{-1} $LiClO_4$–PC, and (d) 1 mol l^{-1} $LiAsF_6$–2Me–THF.

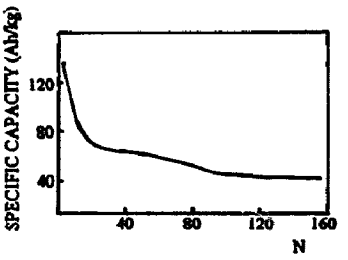

Fig. 6. Cycling capacity of Li/1 mol l^{-1} $LiAsF_6$–PC/$Li_6V_5O_{15}$ cell at charge/discharge rate of 1.0–2.0 mA cm^{-2}, between 3.5 and 1.0 V.

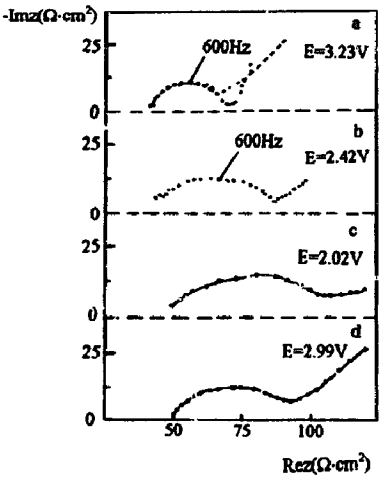

Fig. 7. Complex impedance diagrams of Li/1 mol l^{-1} $LiAsF_6$–PC/$Li_6V_5O_{15}$ cell during discharge and recharge processes (E = cell voltage): (a) before discharge; (b) discharge 1 mAh at 1.0 mA cm^{-1}; (c) discharged 4 mAh at 2.0 mA cm^{-2}, and (d) recharged 2.5 mAh at 2.0 mA cm^{-2}.

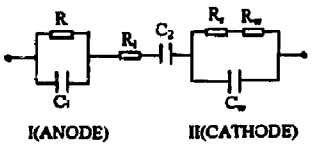

Fig. 8. Equivalent circuit for test cell.

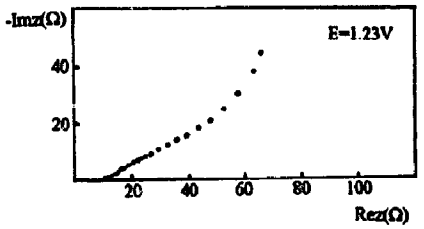

Fig. 9. Complex impedance of $Li_6V_5O_{15}/Li_6V_5O_{15}$, $S = 1.26\ cm^2$; $S_+ = 1.35\ cm^2$; electrolyte = 1 mol l^{-1} $LiAsF_6$–PC.

is displayed in Fig. 7(a) as a dashed line. The coincidence of the a.c. complex impedance data (points in Fig. 7(a)) of the Li/bronze cell before discharge with that of the equivalent circuit confirms that this circuit is reasonable.

During the discharge, the chord length of the high-frequency semi-circle on the real axis increases, while the slope of the curve for the low-frequency part decreases, as shown in Fig. 7(a)–(c). The high-frequency semi-circle relates to the interface resistance of the lithium electrode, and the low-frequency curve relates to the diffusion of lithium in the solid. These results show that the polarization of the cell increases with increasing depth-of-discharge. In addition, the rotating angle of the semicircle (θ) is associated with the roughness of the negative electrode interface and has a tendency to increase with discharge and recharge, which would cause the cell to deteriorate after long cycling.

In order to study the positive-electrode/electrolyte interface reaction, impedance measurements were carried out on a symmetric cell with two $Li_6V_5O_{15}$ electrodes. The a.c. complex impedance plot of the $Li_6V_5O_{15}/Li_6V_5O_{15}$ cell is a line with a slight upturn over the whole frequency range (Fig. 9). This line corresponds to the complex impedance of Li/$Li_6V_5O_{15}$ in the low-frequency range (Fig. 7). Therefore, the high-frequency semi-circles of the Li/$Li_6V_5O_{15}$ cell results from the negative electrode interface. No semi-circles appear in the impedance plot for the symmetric cell. This indicates that the cathode process is controlled by the diffusion of lithium through the bronze, rather than by a simple charge-transfer process [12,13].

4. Conclusions

The new, lithium-rich vanadium bronze $Li_6V_5O_{15}$ has many advantages, such as high capacity (> 340 Ah kg^{-1}), a smooth discharge plateau (1.5 to 1.6 V), a wide charge/discharge range (1.0 to 3.5 V), and outstanding reversibility for lithium intercalation. The new bronze appears to be a good positive electrode material for secondary lithium batteries. X-ray analyses of the charged and discharged products show that the structure of the positive material is stable for lithium insertion, although some rearrangement of the structure possibly occurs. Investigations of the a.c. impedance of Li/$Li_6V_5O_{15}$ cells indicate that the reaction at the positive electrode is limited by lithium diffusion into the lattice of the vanadium bronze.

Acknowledgements

This work was supported by the National Natural Science Foundation of P.R. China.

References

[1] S.N. Hua and X.H. Chen, *Chin. J. Power Sources, 12* (1988) 19.
[2] N. Kumagai, S. Tanifuji and K. Tanno, *J. Power Sources, 35* (1991) 313.
[3] S.N. Hua, G.L. Zhong and Y.Z. Cui, *Chin. J. Power Sources, 18* (1994) 19.
[4] S.P. Panero, M. Pasquali and G. Pistoia, *J. Electrochem. Soc., 130* (1983) 1225.
[5] M. Pasquali, G. Pistoia, V. Manev and R.V. Moshtev, *J. Electrochem. Soc., 133* (1986) 2454.
[6] J.F. Coetzee, *Recommended Methods for Purification of Solvents and Tests for Impurities*, Pergamon, Oxford, 1982.
[7] E.J. Frazer and S. Phang, *J. Power Sources, 10* (1983) 33; S.N. Hua and S. Phang, *J. Power Sources, 10* (1983) 279.
[8] A. Reisman and J. Mineo, *J. Phys. Chem., 66* (1962) 1181.
[9] R. Kohlmuller and J. Martin, *Bull. Soc. Chim. France, 4* (1961) 748.
[10] M. Uchiyama, S. Slane, E. Plichta and M. Salomon, *J. Power Sources, 20* (1987) 279.
[11] R. Mauger, M. Elkordi, J.C. Pariaud, F. Dalard and D. Deroo, *J. Appl. Electrochem., 14* (1984) 293.
[12] N.C. Chaklanabish and H.S. Maito, *J. Power Sources, 16* (1985) 97.
[13] G. Pistoia, M. Pasquali, G. Wang and L. Li, *J. Electrochem. Soc., 137* (1990) 2365.